Front. Phys., 2012, 7(1): 98–108
DOI 10.1007/s11467-011-0216-x

REVIEW ARTICLE

Many-body theories of density response for a strongly correlated Fermi gas

Hui Hu

ARC Centre of Excellence for Quantum-Atom Optics, Centre for Atom Optics and Ultrafast Spectroscopy, Swinburne University of Technology, Melbourne 3122, Australia

E-mail: HHU@groupwise.swin.edu.au

Received September 18, 2011; accepted October 8, 2011

Recent breakthroughs in the creation of ultracold atomic gases in the laboratory have ushered in major changes in physical science. Many novel experiments are now possible, with an unprecedented control of interaction, geometry and purity. Quantum many-body theory is facing severe challenges in quantitatively understanding new experimental results. Here, we review some recently developed theoretical techniques that provide successful predictions for density response of a strongly correlated atomic Fermi gas. These include the strong-coupling random-phase approximation theory, high-temperature quantum virial expansion, and asymptotically exact Tan relations applicable at large momentum.

Keywords quantum many-body theory, Fermi gas

PACS numbers 05.30.Jp, 03.75.Mn, 67.85.Fg, 67.85.Jk

Contents

1 Introduction

Highly correlated systems of fermions are of great interest in a wide range of fields ranging from astrophysics, nuclear physics, condensed matter physics to atomic physics [1, 2]. This great interest comes with an important generic idea of fermionic universality [3, 4]. Any dilute Fermi gases with sufficiently strong interactions should behave identically on a scale given by the average particle separation, independent of the details of the short-ranged interactions. Qualitatively, in a two-component Fermi gas the fermionic universality emerges when the s-wave scattering length a, which characterizes elastic collisions, is much larger than the mean interparticle spacing n^{-3} and the range of the scattering potential r_0 [3], i.e., $a \gg n^{-3} \gg r_0$. When used the Fermi wave-vector $k_{\rm F} = (3\pi^3 n)^{-3}$, this is equivalent to the dimensionless condition of $k_{\rm F}a \gg 1 \gg k_{\rm F}r_0$.

The recently realized ultracold Fermi gases of ^{6}Li and ^{40}K atoms near a broad collisional (Feshbach) resonance appear to be the most appealing systems to study fermionic universality [5]. By taking advantage of the ability to accurately create strong atom–atom attractions with an external magnetic field, the crossover from a Bose–Einstein condensate (BEC) of molecules (atom pairs) to a Bardeen–Cooper–Schrieffer (BCS) superfluid of atoms has now been routinely demonstrated [1, 2]. At the cusp of the crossover, where the s-wave scattering length diverges ($a \to \pm\infty$), atomic Fermi gases should exhibit universal behavior [3]. The Fermi gas in this limit

is referred to as unitary Fermi gas, since its scattering amplitude is unitarily limited. In the extreme BEC and BCS limits, the elementary constitutes of the system are clearly bosons and fermions, respectively. However, in a unitary Fermi gas, bosonic and fermionic excitations play an equally important role. To date, many properties of this new state of matter have been investigated experimentally in harmonically trapped configurations, such as the pairing energy [6], the hydrodynamic expansion [5], the frequency of collective excitations [7–9], the condensate fraction [10, 11], the vortex lattice [12], and the thermodynamic equation of state [13–16].

These novel and important experimental results impose severe challenges for theorists. For a strongly correlated Fermi gas, there is no small interaction parameter to set the accuracy of many-body theories [16, 17]. In recent years, great efforts have been given to developing better quantum Monte Carlo simulations [18–22] and strong-coupling theories [23–26]. A number of static properties, particularly the thermodynamic behavior, have now been understood quantitatively [16]. However, dynamic properties such as the single-particle spectral function [27] and the dynamic density response [28], are not as well understood.

In this paper, we review our recent theoretical progress on understanding the dynamic density response of a strongly correlated atomic Fermi gas. The dynamic density response is characterized by the so-called dynamic structure factor (DSF), which gives the linear response of the many-body system to an excitation process that couples to density [29, 30]. For ultracold atomic gases, it can be conveniently measured by two-photon Bragg spectroscopy using two laser beams [28, 31]. In atomic BECs, density response at small momentum has been measured to characterize the fundamental Bogoliugbov phonon excitations [31]. In ultracold Fermi gases, Bragg spectroscopy has been used to obtain dynamic structure factor over the BEC–BCS crossover [28], albeit at much large momentum.

Our theoretical developments include both perturbative and non-perturbative techniques. At low temperatures, we attempt the conventional random-phase approximation theory [32], which is extended to the strongly interacting crossover regime. At high temperatures, we develope a novel quantum virial expansion method [33]. At large momentum, we derive asymptotically exact results for the structure factor [34], based on the well-known Tan relations [35–37]. All these theories lead to useful predictions that have been quantitatively confirmed by Bragg spectroscopy measurements [38–40].

This review is structured as follows. In the next section, we define DSF and discuss briefly the existing experimental Bragg spectroscopy results. In Section 3, we introduce the random-phase approximation theory and present the comparison of theory to experiment at low temperatures. In Section 4, we describe the quantum virial expansion method and compare the theoretical predictions with experimental data for a unitary Fermi gas at high temperature. In Section 5, we derive exact Tan relations for the structure factor and explain the experimental confirmation of these relations. The last section (Section 6) is devoted to the conclusions and some final remarks.

2 Dynamic structure factor and Bragg spectroscopy

The DSF $S(\boldsymbol{q},\omega)$ is the Fourier transform of the density–density correlation functions at two different space–time points [29, 30]. For a two-component atomic Fermi gas with equal spin populations $N/2$ (referred to as spin-up, $\sigma=\uparrow$, and spin-down, $\sigma=\downarrow$), we have $S_{\uparrow\uparrow}(\boldsymbol{q},\omega)=S_{\downarrow\downarrow}(\boldsymbol{q},\omega)$ and $S_{\uparrow\downarrow}(\boldsymbol{q},\omega)=S_{\downarrow\uparrow}(\boldsymbol{q},\omega)$, each of which is defined by

$$S_{\sigma\sigma'}(\boldsymbol{q},\omega)=Q^{-1}\sum_{nn'}\mathrm{e}^{-\beta E_{n'}}\left\langle n\left|\delta\rho_{\sigma}\left(\boldsymbol{q}\right)\right|n'\right\rangle \times\left\langle n'\left|\delta\rho_{\sigma'}^{\dagger}\left(\boldsymbol{q}\right)\right|n\right\rangle\delta\left(\hbar\omega-E_{nn'}\right) \quad (1)$$

where $|n\rangle$ and $E_{nn'}=E_n-E_{n'}$ are, respectively, the eigenstate and eigenvalue of the many-body system, while $Q=\sum_n\exp(-\beta E_n)\equiv\sum_n\exp[-E_n/(k_{\mathrm{B}}T)]$ is the partition function. The density operator $\delta\hat{\rho}_{\sigma}(\boldsymbol{q})=\sum_{i\sigma}\mathrm{e}^{-\mathrm{i}\boldsymbol{q}\cdot\boldsymbol{r}_i}$ is the Fourier transform of the atomic density operator $\delta\hat{\rho}_{\sigma}(\boldsymbol{r})$ for spin-σ atoms. The total DSF is given by $S(\boldsymbol{q},\omega)\equiv 2[S_{\uparrow\uparrow}(\boldsymbol{q},\omega)+S_{\uparrow\downarrow}(\boldsymbol{q},\omega)]$. The DSF satisfies two remarkable f-sum rules,

$$\int_{-\infty}^{+\infty}S(\boldsymbol{q},\omega)\omega\mathrm{d}\omega=N\frac{\hbar\boldsymbol{q}^2}{2m} \quad (2)$$

and

$$\int_{-\infty}^{+\infty}S_{\uparrow\downarrow}(\boldsymbol{q},\omega)\omega\mathrm{d}\omega=0 \quad (3)$$

where m is the mass of atoms. The exact f-sum rule is important for understanding interacting many-body systems, as it holds irrespective of statistics and temperature.

According to the finite-temperature quantum field theory [29], it is convenient to calculate DSF from dynamic susceptibility, $\chi_{\sigma\sigma'}(\boldsymbol{q},\tau)\equiv-\left\langle T_{\tau}\hat{\rho}_{\sigma}(\boldsymbol{q},\tau)\,\hat{\rho}_{\sigma'}(\boldsymbol{q},0)\right\rangle$, where τ is an imaginary time in the interval $0<\tau\leqslant\beta=1/(k_{\mathrm{B}}T)$. The Fourier component $\chi_{\sigma\sigma'}(\boldsymbol{q},\mathrm{i}\omega_n)$ at discrete Matsubara imaginary frequencies $\mathrm{i}\omega_n=\mathrm{i}2n\pi k_{\mathrm{B}}T$ $(n=0,\pm1,\cdots)$ gives directly the DSF after taking analytic continuation and using the fluctuation–dissipation theorem:

$$S_{\sigma\sigma'}(\boldsymbol{q},\omega)=-\frac{\mathrm{Im}\,\chi_{\sigma\sigma'}(\boldsymbol{q};\mathrm{i}\omega_n\rightarrow\omega+\mathrm{i}0^{+})}{\pi(1-\mathrm{e}^{-\beta\omega})} \quad (4)$$

The frequency integral of the DSF defines the so-called

static structure factor (SSF). For different spin components, we have

$$S_{\sigma\sigma'}(\boldsymbol{q}) = \frac{2}{N}\int_{-\infty}^{+\infty} S_{\sigma\sigma'}(\boldsymbol{q},\omega)\,\mathrm{d}\omega \tag{5}$$

The total SSF is given by, $S(\boldsymbol{q}) = (1/N)\int_{-\infty}^{+\infty}\mathrm{d}\omega S(\boldsymbol{q},\omega) = S_{\uparrow\uparrow}(\boldsymbol{q}) + S_{\uparrow\downarrow}(\boldsymbol{q})$. The SSF is related to the two-body pair correlation function $g_{\sigma\sigma'}(\boldsymbol{r})$ [30]. For the spin-antiparallel SSF, the relation is

$$S_{\uparrow\downarrow}(\boldsymbol{q}) = \frac{N}{2}\int \mathrm{d}\boldsymbol{r}\,[g_{\uparrow\downarrow}(\boldsymbol{r}) - 1]\,\mathrm{e}^{\mathrm{i}\boldsymbol{q}\cdot\boldsymbol{r}} \tag{6}$$

Experimentally, the DSF is measured by inelastic scattering experiments of two-photon Bragg spectroscopy [28, 31]. The atoms are exposed to two laser beams with differences in wave-vector and frequency. In a two-photon scattering event, atoms absorb a photon from one of the beams and emit a photo into the other. Therefore, the difference in the wave-vectors of the beams defines the momentum transfer $\hbar\boldsymbol{q}$, while the frequency difference defines the energy transfer $\hbar\omega$. In the regime of large transferred momentum, which is exactly the case in current experiments for the crossover Fermi gas [28], the single-particle response is dominant and peaks at the quasi-elastic resonance frequency $\omega_{\mathrm{res}} = \hbar\boldsymbol{q}^2/(2M)$, where M is the mass of the elementary constituents of the system. Therefore, we may anticipate that the Bragg response peaks at $\omega_R = \hbar\boldsymbol{q}^2/(2m)$ in the BCS limit and peaks at $\omega_{R,\mathrm{mol}} = \hbar\boldsymbol{q}^2/(4m) = \omega_R/2$ in the BEC limit, since the underlying particles are respectively free atoms ($M = m$) and molecules ($M = 2m$).

In Figs. 1 and 2, we summarize the main experimental results for a harmonically trapped Fermi gas in the BEC–BCS crossover [28, 38–40]. Figure 1 shows the DSF (main panel) and SSF (inset) at several dimensionless interaction strengths and at the lowest experimentally attainable temperature (i.e., $T < 0.1T_{\mathrm{F}}$, where T_{F} is the Fermi temperature) [28], while Fig. 2 presents the

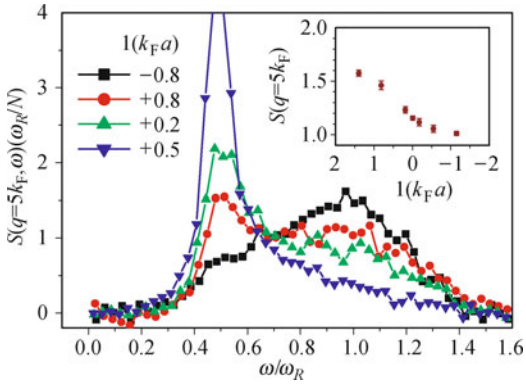

Fig. 1 Measured dynamic structure factor of a harmonically trapped Fermi gas in the BEC–BCS crossover at the lowest attainable temperature ($T < 0.1T_{\mathrm{F}}$) and at a large transferred wave-vector $q = 5k_{\mathrm{F}}$. The inset shows the static structure factor as a function of the dimensionless interaction parameter. Reproduced from Ref. [28], Copyright © 2008 American Physical Society.

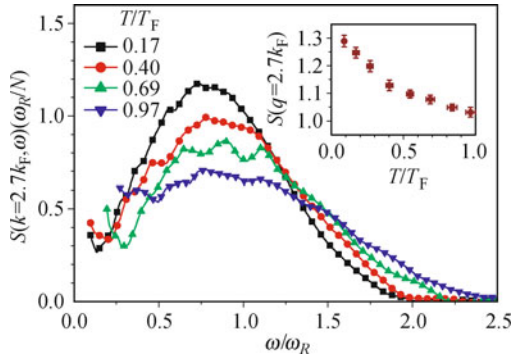

Fig. 2 Temperature dependence of dynamic structure factor of a trapped Fermi gas in the unitary limit, measured at $q = 2.7k_{\mathrm{F}}$. The inset shows the temperature dependence of static structure factor. Reproduced from Refs. [39] and [40], Copyright © 2011 American Physical Society and Copyright © 2011 Institute of Physics respectively.

temperature dependence of structure factors in the most interesting unitary limit [39, 40]. As anticipated, in Fig. 1, the DSF peaks at $\omega_R/2$ and ω_R on the BEC side (i.e., $1/(k_{\mathrm{F}}a) = +0.5$) and on the BCS side [$1/(k_{\mathrm{F}}a) = -0.8$], respectively. In the unitary limit, where the statistics of the elementary excitations is not well defined, we observe a two-peak structure with responses from both molecules and free-atoms. As the temperature increases (Fig. 2), however, these two peaks emerge. The resultant broad peak shifts eventually to ω_R at high temperatures.

The appearance of a molecular response in the BEC-BCS crossover is also captured by the SSF. As shown in the insets of both figures, with increasing interaction strength or temperature, the SSF increases from 1 to 2. This can be understood from the f-sum rule. By assuming that the response is exhausted by a single-mode excitation at $\omega_{\mathrm{res}} = \hbar\boldsymbol{q}^2/(2M)$, the f-sum rule can be rewritten by

$$N\frac{\hbar\boldsymbol{q}^2}{2m} = \int_{-\infty}^{+\infty} S(\boldsymbol{q},\omega)\omega\mathrm{d}\omega \approx NS(\boldsymbol{q})\,\omega_{\mathrm{res}} \tag{7}$$

Therefore, we obtain $S(\boldsymbol{q}) = M/m$, which should change from 1 to 2 through the crossover. In other words, we may regard $mS(\boldsymbol{q})$ as the effective mass of the elementary constituents of the system.

3 Strong-coupling random-phase approximation theory

In this section, we extend a perturbative random-phase approximation (RPA) theory to strongly interacting regime and use it to describe *quantitatively* the observed low-temperature Bragg spectra for harmonically *trapped* ^{6}Li atoms at large transferred momenta (see Fig. 1) [32]. The RPA method has previously been applied to study the DSF [42] and collective oscillations [43] of weakly interacting Fermi superfluids. A dynamic mean-field approach [41, 44], identical to the RPA but based on kinetic

equations, was developed to investigate structure factors and collective modes of a uniform, strongly interacting Fermi gas.

3.1 The basic idea of RPA theory

To outline briefly the central idea of RPA, we consider the single-channel Hamiltonian [45],

$$\mathcal{H}=\sum_{\sigma}\int \mathrm{d}\boldsymbol{r}\psi_{\sigma}^{+}(\boldsymbol{r})\left[-\frac{\hbar^{2}\nabla^{2}}{2m}-\mu+V_{T}(\boldsymbol{r})\right]\psi_{\sigma}(\boldsymbol{r}) +U_{0}\int \mathrm{d}\boldsymbol{r}\psi_{\uparrow}^{+}(\boldsymbol{r})\psi_{\downarrow}^{+}(\boldsymbol{r})\psi_{\downarrow}(\boldsymbol{r})\psi_{\uparrow}(\boldsymbol{r}) \tag{8}$$

which describes a balanced spin-1/2 Fermi gas in a harmonic trap $V_T(\boldsymbol{r})$, where fermions with unlike spins interact via a contact potential $U_0\delta(\boldsymbol{r}-\boldsymbol{r}')$. The total number of atoms N is tuned by the chemical potential μ and the bare interaction strength U_0 is renormalized by the s-wave scattering length,

$$\frac{1}{U_0}+\sum_{\boldsymbol{k}}\frac{m}{\hbar^{2}\boldsymbol{k}^{2}}=\frac{m}{4\pi\hbar^{2}a} \tag{9}$$

In the superfluid phase, we treat the system as a gas of long-lived Bogoliubov quasiparticles interacting through a mean-field and consider its response to a weak external field of the form of $\delta V\mathrm{e}^{\mathrm{i}(\boldsymbol{q}\cdot\boldsymbol{r}-\omega t)}$. The essential idea of the RPA is that there is a self-generated mean-field potential experienced by quasiparticles, associated with the local changes in the density distribution of the two spin species, $\delta U=U_0\int \mathrm{d}\boldsymbol{r}(\sum_{\sigma}\delta n_{\sigma}\psi_{\sigma}^{+}\psi_{\sigma}+\delta m\psi_{\uparrow}^{+}\psi_{\downarrow}^{+}+\delta m^{*}\psi_{\downarrow}\psi_{\uparrow})$, where $\delta n_{\sigma}\equiv\delta n_{\sigma}(\boldsymbol{r},t)$ and $\delta m\equiv\delta m(\boldsymbol{r},t)$ are the normal and anomalous density fluctuations, respectively, which must be determined self-consistently [42, 43, 46, 47]. In the linear approximation, the self-generated potential δU plays the same role as the perturbation field when we calculate the dynamic response using a static BCS Hamiltonian as the reference system. This leads to coupled equations for density fluctuations. The linear response is characterized by a matrix consisting of all two-particle response functions [43]:

$$\chi\equiv\begin{pmatrix}\langle\langle\hat{n}_{\uparrow}\hat{n}_{\uparrow}\rangle\rangle & \langle\langle\hat{n}_{\uparrow}\hat{n}_{\downarrow}\rangle\rangle & \langle\langle\hat{n}_{\uparrow}\hat{m}\rangle\rangle & \langle\langle\hat{n}_{\uparrow}\hat{m}^{+}\rangle\rangle\\ \langle\langle\hat{n}_{\downarrow}\hat{n}_{\uparrow}\rangle\rangle & \langle\langle\hat{n}_{\downarrow}\hat{n}_{\downarrow}\rangle\rangle & \langle\langle\hat{n}_{\downarrow}\hat{m}\rangle\rangle & \langle\langle\hat{n}_{\downarrow}\hat{m}^{+}\rangle\rangle\\ \langle\langle\hat{m}\hat{n}_{\uparrow}\rangle\rangle & \langle\langle\hat{m}\hat{n}_{\downarrow}\rangle\rangle & \langle\langle\hat{m}\hat{m}\rangle\rangle & \langle\langle\hat{m}\hat{m}^{+}\rangle\rangle\\ \langle\langle\hat{m}^{+}\hat{n}_{\uparrow}\rangle\rangle & \langle\langle\hat{m}^{+}\hat{n}_{\downarrow}\rangle\rangle & \langle\langle\hat{m}^{+}\hat{m}\rangle\rangle & \langle\langle\hat{m}^{+}\hat{m}^{+}\rangle\rangle\end{pmatrix} \tag{10}$$

where $\langle\langle\hat{A}\hat{B}\rangle\rangle$ is the Fourier transform of the retarded function $-\mathrm{i}\Theta(t-t')\langle[\hat{A}(\boldsymbol{r},t),\hat{B}(\boldsymbol{r}',t')]\rangle$. For simplicity, we abbreviate $\chi_{\sigma\sigma'}\equiv\langle\langle\hat{n}_{\sigma}\hat{n}_{\sigma'}\rangle\rangle$, $\chi_{\sigma m}\equiv\langle\langle\hat{n}_{\sigma}\hat{m}\rangle\rangle$, $\chi_{\sigma\bar{m}}\equiv\langle\langle\hat{n}_{\sigma}\hat{m}^{+}\rangle\rangle$, $\chi_{m\bar{m}}\equiv\langle\langle\hat{m}\hat{m}^{+}\rangle\rangle$, and so on. By solving the coupled equations for density fluctuations, the standard RPA response function χ can be expressed in terms of the static BCS response function χ^0 [43],

$$\chi=\chi^{0}\left(\hat{1}-U_{0}\chi^{0}\mathcal{G}\right)^{-1} \tag{11}$$

where $\mathcal{G}=\delta(\boldsymbol{r}-\boldsymbol{r}')(\sigma_0\otimes\sigma_x)$ is a direct product of two Pauli matrices σ_0 and σ_x and the unit matrix $\hat{1}=\delta(\boldsymbol{r}-\boldsymbol{r}')(\sigma_0\otimes\sigma_0)$. The dynamic structure factor $S_{\sigma\sigma'}(\omega)$ is then obtained by using the fluctuation–dissipation theorem Eq. (4). In the weak-coupling regime, Eq. (11) has been solved by calculating χ^0 for a thermal average of BCS quasiparticles [42, 43].

3.2 Strong-coupling RPA theory

Here, we extend the RPA to the strongly interacting regime with an arbitrarily large scattering length a, by properly renormalizing the bare interaction strength U_0 and the two response functions $\chi^0_{m\bar{m}}$ and $\chi^0_{\bar{m}m}$, which was found to be suitable at the BEC–BCS crossover [32]. The ultraviolet divergence of these two functions is canceled exactly by the small value of U_0, when the momentum cut-off goes to infinity. In homogeneous systems, a careful account of the divergent terms in the inverted matrix of the RPA equation (11) leads to a concise expression for the response functions:

$$\chi_{\uparrow\uparrow}=\chi^{0}_{\uparrow\uparrow}-\left[2\chi^{0}_{\uparrow\downarrow}\chi^{0}_{\uparrow m}\chi^{0}_{\uparrow\bar{m}}+\left(\chi^{0}_{\uparrow m}\right)^{2}\tilde{\chi}^{0}_{m\bar{m}} +\left(\chi^{0}_{\uparrow\bar{m}}\right)^{2}\tilde{\chi}^{0}_{\bar{m}m}\right]/\left[\tilde{\chi}^{0}_{m\bar{m}}\tilde{\chi}^{0}_{\bar{m}m}-\left(\chi^{0}_{\uparrow\downarrow}\right)^{2}\right] \tag{12}$$

and

$$\chi_{\uparrow\downarrow}=\chi_{\uparrow\uparrow}-\chi^{0}_{\uparrow\uparrow}+\chi^{0}_{\uparrow\downarrow} \tag{13}$$

where the response functions with a tilde, i.e., $\tilde{\chi}^{0}_{m\bar{m}}\equiv\chi^{0}_{m\bar{m}}+\sum_{\boldsymbol{k}}m/(\hbar^{2}\boldsymbol{k}^{2})-m/(4\pi\hbar^{2}a)$, become free from any ultraviolet divergence. Note that, we use a Leggett–BCS ground state without inclusion of the Hartree–Fock term in the quasiparticle spectrum. Therefore, in the BCS regime our treatment does not account for the leading interaction effect. At the crossover, however, it does capture the dominant pairing gap. Note also that, the RPA method accounts for single particle–hole excitations. Higher correlations such as multi-particle–hole excitations are neglected.

In the presence of a harmonic trap, the renormalization procedure becomes cumbersome because of the discrete energy levels. It is convenient to use a local density approximation (LDA) [48, 49], which treats the system as a collection of many homogeneous cells with local chemical potential, $\mu(\boldsymbol{r})=\mu-V_T(\boldsymbol{r})$, where $V_T(\boldsymbol{r})=M(\omega_x^2x^2+\omega_y^2y^2+\omega_z^2z^2)/2$ is the harmonic trapping potential. The LDA treatment is valid for a large number of atoms such as $N\sim10^5$ as in experiments. At a given temperature and scattering length, we solve the Leggett–BCS equation with local chemical potential for the local pairing gap and calculate the static response function χ^0, then solve the local RPA density response functions using Eqs. (12) and (13), and finally obtain the total

RPA responses by integrating over the whole trap. To calculate the dimensionless interaction strength $1/(k_{\rm F}a)$, we use the Fermi wave-vector $k_{\rm F} = \sqrt{2mE_{\rm F}/\hbar^2}$ at the trap center, where the trapped Fermi energy is given by $E_{\rm F} = \hbar(3N\omega_x\omega_y\omega_z)^{1/3}$ [2].

3.3 Comparison of theory with experiment at zero temperature

Figure 3 shows the zero-temperature spin parallel, anti-parallel, and total DSF at a transferred wave-vector $q = 5k_{\rm F}$ in the BEC–BCS crossover, calculated using the above RPA procedure for a trapped Fermi gas [32]. In addition to a broad response at the atomic resonance frequency $\omega_R = \hbar q^2/(2M) = 25E_{\rm F}/\hbar$ caused by resonant scattering of atoms, a much narrower peak develops at about $\omega_R/2$ with increased coupling. This is precisely what has been observed in the Bragg spectroscopy experiment. Physically, it is the Bogoliubov–Anderson phonon mode of a Fermi superfluid at large wave-vectors, which evolves continuously into a Bogoliubov mode of molecules towards the BEC limit [41]. The molecular peak is mostly evident in $S_{\uparrow\downarrow}$ as there is no background atomic response.

To make a quantitative comparison with the experimental spectra, we take into account the spectral broadening due to the finite experimental Bragg pulse duration ($\tau_{\rm Br} = 40$ μs) [28]. We calculate theoretically,

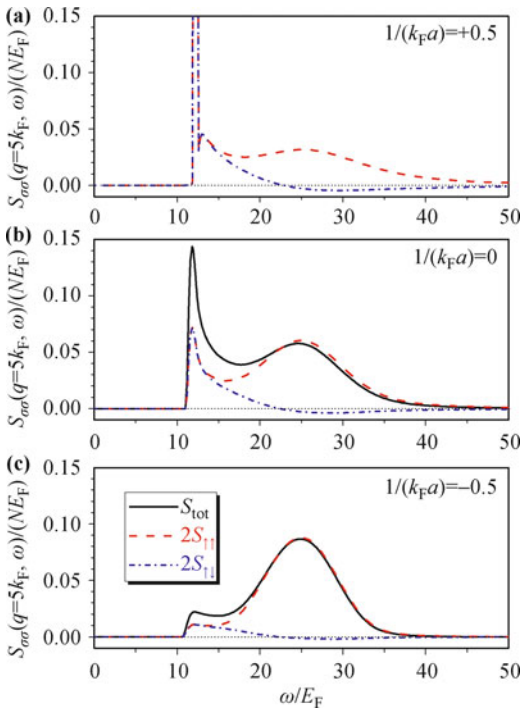

Fig. 3 Zero temperature spin parallel $S_{\uparrow\uparrow}(\boldsymbol{q},\omega)$ (*dashed lines*), anti-parallel $S_{\uparrow\downarrow}(\boldsymbol{q},\omega)$ (*dot-dashed lines*), and total dynamic structure factor $S(\boldsymbol{q},\omega) = 2[S_{\uparrow\uparrow}+S_{\uparrow\downarrow}]$ (*solid lines*) across the BEC–BCS crossover: $1/(k_{\rm F}a) = 0.5$ (**a**), 0.0 (**b**), and -0.5 (**c**). The negative weight in $S_{\uparrow\downarrow}$ at about the atomic resonance frequency is consistent with the exact sum rule $\int \omega S_{\uparrow\downarrow}(\mathbf{q},\omega){\rm d}\omega = 0$. Reproduced from Ref. [32], Copyright © 2010 American Physical Society.

$$S_{\rm expt}(\boldsymbol{q},\omega) \propto \frac{1}{\pi\sigma}\int_{-\infty}^{\infty} {\rm d}\omega' S(\boldsymbol{q},\omega'){\rm sinc}^2\frac{\omega-\omega'}{\sigma} \qquad (14)$$

where ${\rm sinc}\, x = (\sin x)/x$ and the energy resolution $\sigma = 2/\tau_{\rm Br}$. We find $\sigma \approx 0.68E_{\rm F} \approx 0.027\omega_R$. Figure 4 presents a comparison of the experimental data (open squares) with the RPA predictions (lines) for the Bragg spectra. Without any free parameters, our RPA predictions agree well with the experimental results in the unitarity regime [$1/(k_{\rm F}a) = 0.0$ and 0.2] and BEC regime [$1/(k_{\rm F}a) = 0.8$]. The agreement on the BCS side [$1/(k_{\rm F}a) = -0.5$], however, becomes a bit worse. The quantitative agreement around unitarity is very compelling, since the RPA was assumed to be unreliable in the (strongly interacting) regime of large pair fluctuations. Our comparison indicates that the RPA is able to describe the dynamical properties of the BEC–BCS crossover, at least at zero temperature and large momenta. High order multi-particle–hole excitations, absent in the RPA theory, seems to be negligibly small at large momenta. The somewhat poorer agreement at $1/(k_{\rm F}a) = -0.5$ can be attributed to the mean-field shift, which is ignored in the RPA but dominates for sufficiently weak interactions.

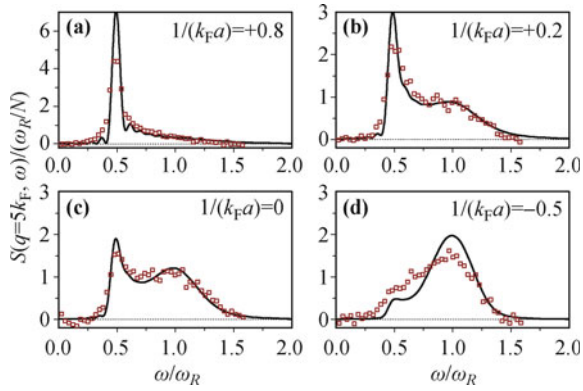

Fig. 4 Quantitative comparison of theoretical and experimental Bragg spectra. The RPA prediction (*lines*) agrees well with the experimental data (*empty squares*) [28] at the BEC–BCS crossover, with no free parameters. Reproduced from Ref. [32], Copyright © 2010 American Physical Society.

The good agreement between the RPA theory and the Bragg experiment is further confirmed by comparing the SSF at zero temperature, as reported in Fig. 5. Note that, the measured SSF is not affected by the spectral broadening due to the finite Bragg pulse duration. It is evident that the RPA prediction (plus symbols) fits very well with the experimental data (solid circles). We also show an independent theoretical prediction from exact Tan relations, which will be discussed in detail in Section 5. The two theoretical predictions agree well with each other.

4 Quantum cluster expansion

Let us now consider the non-perturbative quantum virial

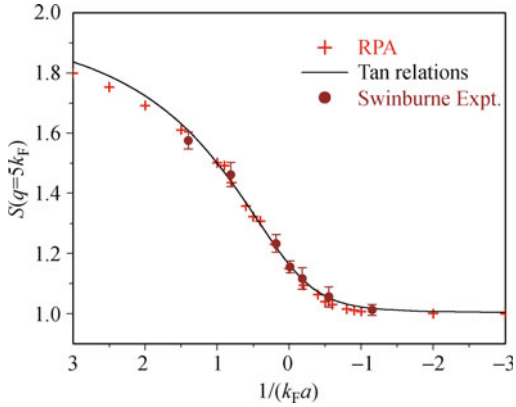

Fig. 5 Quantitative comparison between theory and experiment for the zero temperature static structure factor across the crossover. With no free parameters, our RPA prediction (*plus symbols*) agrees well with the experimental data for $S(\boldsymbol{q})$ (*solid circles with error bars*) [38] and an independent theoretical result based on the exact Tan relations (*solid line*). Reproduced from Ref. [32], Copyright © 2010 American Physical Society.

expansion [33]. Virial expansion has proved to be an efficient method for studying the high-temperature properties of ultracold atomic Fermi gases [16, 50–55]. This method utilizes the fact that in the high temperature limit, the chemical potential μ diverges to $-\infty$ and the fugacity $z \equiv \exp[\mu/(k_{\mathrm{B}}T)] \ll 1$ is a well-defined small expansion parameter. Thus, one may expand any physical quantities of interest in powers of fugacity, no matter how strong the interactions.

4.1 Virial expansion of DSF

We construct first the virial expansion for the dynamic susceptibility $\chi_{\sigma\sigma'}(\boldsymbol{r},\boldsymbol{r}';\tau>0)$, which is given by

$$\chi_{\sigma\sigma'} \equiv -\frac{\mathrm{Tr}\left[\mathrm{e}^{-\beta(\mathcal{H}-\mu\mathcal{N})}\mathrm{e}^{\mathcal{H}\tau}\hat{n}_\sigma(\boldsymbol{r})\,\mathrm{e}^{-\mathcal{H}\tau}\hat{n}_{\sigma'}(\boldsymbol{r}')\right]}{\mathrm{Tr}\mathrm{e}^{-\beta(\mathcal{H}-\mu\mathcal{N})}} \quad (15)$$

At high temperatures, Taylor-expanding in terms of the powers of small fugacity $z \equiv \exp[\mu/(k_{\mathrm{B}}T)] \ll 1$ leads to $\chi_{\sigma\sigma'}(\boldsymbol{r},\boldsymbol{r}';\tau) = (zX_1 + z^2X_2 + \cdots)/(1 + zQ_1 + z^2Q_2 + \cdots) = zX_1 + z^2(X_2 - X_1Q_1) + \cdots$, where we have introduced the cluster functions $X_n = -\mathrm{Tr}_n[\mathrm{e}^{-\beta\mathcal{H}}\mathrm{e}^{\tau\mathcal{H}}\hat{n}_\sigma(\boldsymbol{r})\mathrm{e}^{-\tau\mathcal{H}}\hat{n}_{\sigma'}(\boldsymbol{r}')]$ and $Q_n = \mathrm{Tr}_n\mathrm{e}^{-\beta\mathcal{H}}$, with n denoting the number of particles in the cluster and Tr_n denoting the trace over n-particle states of proper symmetry. We shall refer to the above expansion as the virial expansion of dynamic susceptibilities, $\chi_{\sigma\sigma'}(\boldsymbol{r},\boldsymbol{r}';\tau) = z\chi_{\sigma\sigma',1}(\boldsymbol{r},\boldsymbol{r}';\tau) + z^2\chi_{\sigma\sigma',2}(\boldsymbol{r},\boldsymbol{r}';\tau) + \cdots$, where

$$\begin{aligned}\chi_{\sigma\sigma',1}(\boldsymbol{r},\boldsymbol{r}';\tau) &= X_1\\ \chi_{\sigma\sigma',2}(\boldsymbol{r},\boldsymbol{r}';\tau) &= X_2 - X_1Q_1, \text{ etc.}\end{aligned} \quad (16)$$

Accordingly, we shall write for the dynamic structure factors

$$S_{\sigma\sigma'}(\boldsymbol{q},\omega) = zS_{\sigma\sigma',1}(\boldsymbol{q},\omega) + z^2S_{\sigma\sigma',2}(\boldsymbol{q},\omega) + \cdots \quad (17)$$

The calculation of the n-th expansion coefficient requires the knowledge of all solutions up to n-body, including both the eigenvalues and eigenstates [51, 52]. Here we aim to calculate the leading effect of interactions, which contribute to the 2nd-order expansion function [33]. For this purpose, it is convenient to define $\Delta\chi_{\sigma\sigma',2} \equiv \{\chi_{\sigma\sigma',2}\}^{(I)} = \{X_2\}^{(I)}$ and $\Delta S_{\sigma\sigma',2} \equiv \{S_{\sigma\sigma',2}\}^{(I)}$. The notation $\{\ \}^{(I)}$ means the contribution due to interactions inside the bracketed term, so that $\{X_2\}^{(I)} = X_2 - X_2^{(1)}$, where the superscript "1" in $X_2^{(1)}$ denotes quantities for a noninteracting system. We note that the inclusion of the 3rd-order expansion function is straightforward, though involving more numerical effort.

It is easy to see that $\Delta\chi_{\sigma\sigma',1} = 0$, according to the definition of notation $\{\ \}^{(I)}$. To calculate the 2nd-order expansion function for the dynamic susceptibility, $\Delta\chi_{\sigma\sigma',2} = -\left\{\mathrm{Tr}_{\uparrow\downarrow}\left[\mathrm{e}^{-\beta\mathcal{H}}\mathrm{e}^{\tau\mathcal{H}}\hat{n}_\sigma(\boldsymbol{r})\,\mathrm{e}^{-\tau\mathcal{H}}\hat{n}_{\sigma'}(\boldsymbol{r}')\right]\right\}^{(I)}$, we insert the identity $\sum_Q |Q\rangle\langle Q| = \hat{\mathbf{1}}$ and take the trace over the state P, i.e., $\Delta\chi_{\sigma\sigma',2} = -\sum_{P,Q}\left[\mathrm{e}^{-\beta E_P+\tau(E_P-E_Q)}\langle P|\hat{n}_\sigma|Q\rangle\langle Q|\hat{n}_{\sigma'}|P\rangle\right]^{(I)}$. Here, P and Q are the two-atom eigenstates with energies E_P and E_Q, respectively. Expressing the density operator in the first quantization: $\hat{n}_\uparrow(\boldsymbol{r}) = \sum_i \delta(\boldsymbol{r}-\boldsymbol{r}_{i\uparrow})$ and $\hat{n}_\downarrow(\boldsymbol{r}) = \sum_j \delta(\boldsymbol{r}-\boldsymbol{r}_{j\downarrow})$, it is straightforward to show that

$$\Delta\chi_{\sigma\sigma',2} = -\sum_{P,Q}\left[\mathrm{e}^{-\beta E_P+\tau(E_P-E_Q)}C^{PQ}_{\sigma\sigma'}(\boldsymbol{r},\boldsymbol{r}')\right]^{(I)} \quad (18)$$

where

$$C^{PQ}_{\uparrow\uparrow} \equiv \int \mathrm{d}\boldsymbol{r}_2\mathrm{d}\boldsymbol{r}_2'\left[\Phi_P^*\Phi_Q\right](\boldsymbol{r},\boldsymbol{r}_2)\left[\Phi_Q^*\Phi_P\right](\boldsymbol{r}',\boldsymbol{r}_2') \quad (19)$$

and

$$C^{PQ}_{\uparrow\downarrow} \equiv \int \mathrm{d}\boldsymbol{r}_1\mathrm{d}\boldsymbol{r}_2[\Phi_P^*\Phi_Q](\boldsymbol{r},\boldsymbol{r}_2)\left[\Phi_Q^*\Phi_P\right](\boldsymbol{r}_1,\boldsymbol{r}') \quad (20)$$

The dynamic structure factor can be obtained by taking the analytic continuation. This result is $\Delta S_{\sigma\sigma',2}(\boldsymbol{r},\boldsymbol{r}';\omega) = \sum_{P,Q}\left[\delta(\omega+E_P-E_Q)\,\mathrm{e}^{-\beta E_P}C^{PQ}_{\sigma\sigma'}(\boldsymbol{r},\boldsymbol{r}')\right]^{(I)}$. Applying a further Fourier transform with respect to $\boldsymbol{x} = \boldsymbol{r}-\boldsymbol{r}'$ and integrating over $\boldsymbol{R} = (\boldsymbol{r}+\boldsymbol{r}')/2$, we obtain the response $\Delta S_{\sigma\sigma',2}(\boldsymbol{q},\omega)$,

$$\Delta S_{\sigma\sigma',2} = \sum_{P,Q}\left[\delta(\omega+E_P-E_Q)\,\mathrm{e}^{-\beta E_P}F^{PQ}_{\sigma\sigma'}(\boldsymbol{q})\right]^{(I)} \quad (21)$$

where $F^{PQ}_{\sigma\sigma'}(\boldsymbol{q}) = \int \mathrm{d}\boldsymbol{r}\mathrm{d}\boldsymbol{r}'\mathrm{e}^{-\mathrm{i}\boldsymbol{q}\cdot(\boldsymbol{r}-\boldsymbol{r}')}C^{PQ}_{\sigma\sigma'}(\boldsymbol{r},\boldsymbol{r}')$.

The calculation of $C^{PQ}_{\sigma\sigma'}(\boldsymbol{r},\boldsymbol{r}')$ or $F^{PQ}_{\sigma\sigma'}(\boldsymbol{q})$ is straightforward but tedious, by using the two-atom solutions in an isotropic harmonic trap $m\omega_0^2r^2/2$. We refer to Ref. [33] for details. The final result is given by

$$\Delta S_{\sigma\sigma',2} = B\sqrt{\frac{m}{\pi}}\sum_{p2q2}\left[\mathrm{e}^{-\frac{\beta(\tilde{\omega}+\epsilon_{p2}-\epsilon_{q2})^2}{2\omega_R}}\mathrm{e}^{-\beta\epsilon_{p2}}A^{\sigma\sigma'}_{p2q2}\right]^{(I)} \quad (22)$$

where $B \equiv (k_{\rm B}T)^{5/2}/(q\hbar^4\omega_0^3)$, $\tilde{\omega} = \omega - \omega_R/2$, and

$$A^{\sigma\sigma'}_{p2q2} = (-1)^{l(1-\delta_{\sigma\sigma'})}(2l+1) \times \left[\int_0^\infty {\rm d}x x^2 j_l\left(\frac{qx}{2}\right)\phi_{n_p l_p}(x)\,\phi_{n_q l_q}(x)\right]^2 \quad (23)$$

In Eq. (23), we specify $p2 = \{n_p l_p\}$ and $q2 = \{n_q l_q\}$, and $l = \max\{l_p, l_q\}$ for the two-atom relative radial wave functions ϕ with energy ϵ. We require that either l_p or l_q should be zero (i.e., $\min\{l_p, l_q\} = 0$), otherwise, $A^{\sigma\sigma'}_{p2q2}$ will be cancelled exactly by the non-interacting terms.

Together with the non-interacting DSF $S^{(1)}_{\sigma\sigma'}$, we calculate directly the interacting structure factor,

$$S_{\sigma\sigma'}(\boldsymbol{q},\omega) = S^{(1)}_{\sigma\sigma'}(\boldsymbol{q},\omega) + z^2\Delta S_{\sigma\sigma',2} \quad (24)$$

once the fugacity z is determined by the virial expansion for equation of state.

4.2 Comparison of theory with experiment at high temperatures

Considerable insight into the dynamic structure factor of a strongly correlated Fermi gas can already be seen from Eq. (22), in which the spectrum is peaked roughly at $\omega_{R,\rm mol} = \omega_R/2$, the resonant frequency for molecules. Therefore, the peak is related to the response of molecules with the mass $M = 2m$. Equation (22) shows clearly how the molecular response develops with the modified two-fermion energies and wave functions as the interaction strength increases. In the BCS limit where $\Delta S_{\sigma\sigma',2}$ is small, the response is determined by the non-interacting background $S^{(1)}_{\sigma\sigma'}$ that peaks at ω_R. In the extreme BEC limit ($a \to 0^+$), however, $\Delta S_{\sigma\sigma',2}$ dominates. The sum in $\Delta S_{\sigma\sigma',2}$ is exhausted by the (lowest) tightly bound state $\phi_{\rm rel}(x) \simeq \sqrt{2/a}{\rm e}^{-x/a}$ with energy $\epsilon_{\rm rel} \simeq -\epsilon_B \equiv -\hbar^2/(ma^2)$. The chemical potential of molecules is given by $\mu_m = 2\mu + \epsilon_B$. Therefore, the DSF of fermions takes the form of

$$S^{\rm BEC}_{\sigma\sigma'} \simeq z_m B\sqrt{\frac{M}{\pi}}\exp\left[-\frac{\beta(\omega-\omega_{R,\rm mol})^2}{4\omega_{R,\rm mol}}\right] \quad (25)$$

where $z_m = {\rm e}^{\beta\mu_m}$ is the molecular fugacity. This peaks at the molecular resonant energy. As anticipated, Eq. (25) is exactly the leading virial expansion term in the DSF of non-interacting molecules. It is clear that $S_{\uparrow\uparrow}(\boldsymbol{q},\omega) \simeq S_{\uparrow\downarrow}(\boldsymbol{q},\omega)$ in the BEC limit, since the spin structure in a single molecule can no longer be resolved.

To understand the intermediate regime, in Fig. 6(a) we report numerical results for the DSF as the interaction strength increases from the BCS to BEC regimes at $T = 0.5T_{\rm F}$ [33]. The temperature dependence of the DSF in the unitary limit is shown in Fig. 6(b) [32]. In a trapped gas with total number of fermions N, we use the zero temperature Thomas–Fermi wave vector $k_{\rm F} = (24N)^{1/6}/a_{ho}$ and temperature $T_{\rm F} = (3N)^{1/3}\hbar\omega_0/k_{\rm B}$ as characteristic units. In accord with the experiment [28, 39], we take a large transferred momentum of $q = 3k_{\rm F}$. At $T = 0.5T_{\rm F}$, a smooth transition from atomic to molecular responses is evident as the interaction parameter $1/(k_{\rm F}a)$ increases, in qualitative agreement with the experimental observation (c.f. Fig. 1). In the unitary limit, the peak of total DSF shifts towards the molecular recoil frequency, as indicated by the dark circles. This red-shift is again in qualitative agreement with the experiment (c.f. Fig. 2).

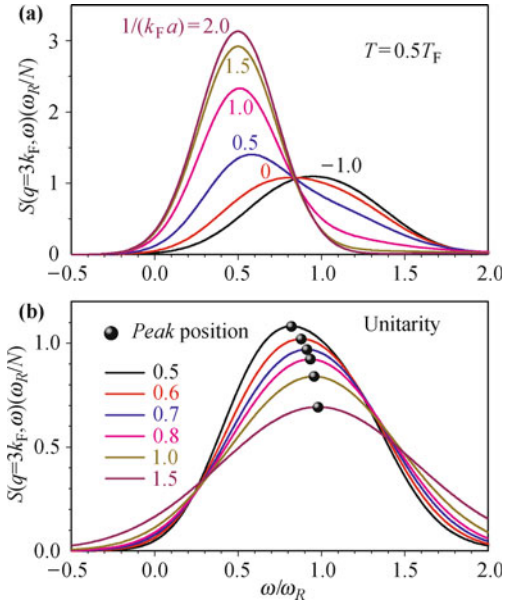

Fig. 6 (**a**) Evolution of dynamic structure factor of a trapped Fermi gas in the BEC–BCS crossover with increasing interaction strength $1/(k_{\rm F}a)$ at $T = 0.5T_{\rm F}$. (**b**) Temperature dependence of dynamic structure factor of a trapped unitary Fermi gas. The dark circles indicate the peak position of the spectra. The transferred wave-vector is $q = 3k_{\rm F}$. Reproduced from Ref. [33], Copyright © 2010 American Physical Society.

For a close comparison, we plot in Fig. 7 the virial expansion prediction and experimental data for the DSF at several temperatures in the unitary limit. The theory is in very good agreement with experimental data at high temperatures (i.e., $T = 0.97T_{\rm F}$ and $T = 0.69T_{\rm F}$) [39, 40], where the fugacity z is less than 1. Towards low temperatures, the agreement becomes worse. However, the virial expansion does capture the qualitative feature of the DSF for temperature down to the superfluid transition temperature $T_c \sim 0.2T_{\rm F}$.

5 Exact Tan relations

In this section, we present an exact relation for the large-momentum behavior of the spin-antiparallel static structure factor $S_{\uparrow\downarrow}(q)$, showing that it has a simple universal power-law $(1/q)$ tail [34]. The relation we consider, hereafter referred to as the structure-factor Tan relation, belongs to the family of exact relations obtained by Shina Tan in 2005 [35–37], which link the short-range,

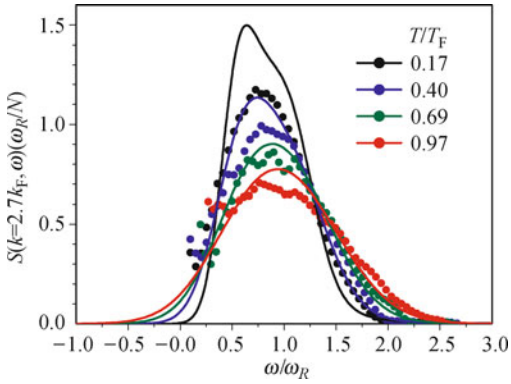

Fig. 7 Comparison between theory and experiment for the dynamic structure factor of a trapped unitary Fermi gas at finite temperatures. Here, the transferred wave-vector is $q = 2.7k_F$. Reproduced from Ref. [40], Copyright © 2011 Institute of Physics.

large-momentum, and high-frequency asymptotic behavior of many-body systems to their thermodynamic properties. For instance, the momentum distribution [35–37] and RF-spectroscopy [56, 57] fall off as q^{-4} and $\omega^{-5/2}$, respectively. All the Tan relations are related to each other by a single coefficient $\mathcal{I}$, referred to as the integrated contact density or contact. The contact measures the probability of two fermions with unlike spins being close together [58]. It also links the short-range behavior to thermodynamics via the adiabatic relation [35–37], $\mathrm{d}E/\mathrm{d}(-1/a) = \hbar^2\mathcal{I}/(4\pi m)$, which gives the change in the total energy E due to adiabatic changes in the scattering length. The fundamental importance of the Tan relations arises from their wide applicability. They are useful at both zero or finite temperature, superfluid or normal phase, homogeneous or trapped, few-body or many-body systems.

We also consider the large-frequency tail of the DSF at large momentum [59]. By using Feynman diagrams, we show that the spin parallel and antiparallel DSFs have respectively a tail of the form $\sim \pm\omega^{-5/2}$ for $\omega \to \infty$, decaying slower than the total DSF found previously ($\sim \omega^{-7/2}$) [60, 61].

5.1 The structure-factor Tan relation

The structure factor Tan relation for $S_{\uparrow\downarrow}(q)$ follows directly from the short-range behavior of the pair correlation function $g_{\uparrow\downarrow}(\boldsymbol{r}) \equiv \int \mathrm{d}\boldsymbol{R}\langle\hat{\rho}_\uparrow(\boldsymbol{R}-\boldsymbol{r}/2)\,\hat{\rho}_\downarrow(\boldsymbol{R}+\boldsymbol{r}/2)\rangle$, which diverges as [35–37]

$$g_{\uparrow\downarrow}(\boldsymbol{r}\to 0) \simeq \frac{\mathcal{I}}{16\pi^2}\left(\frac{1}{r^2}-\frac{2}{ar}\right) \tag{26}$$

A Fourier transformation of $g_{\uparrow\downarrow}(\boldsymbol{r}\to 0)$ then leads to [34]

$$S_{\uparrow\downarrow}(q \gg k_F) \simeq \frac{\mathcal{I}}{4Nq}\left(1-\frac{4}{\pi aq}\right) \equiv \frac{\mathcal{I}}{Nk_F}t(q) \tag{27}$$

where k_F is the Fermi wave-vector and N is the total number of atoms. On the right hand side of the above equation, we have defined $t(q) \equiv [k_F/(4q)][1-4/(\pi aq)]$. Equation (27) holds in a scaling region of sufficiently large q near the unitarity limit ($a \to \pm\infty$) so that the next-order correction in the bracket [$\propto 1/(aq)$] is small compared to the leading term of 1.

The power-law tail of $1/q$ in the structure-factor relation is more amenable for experimental investigation than the q^{-4} or $\omega^{-5/2}$ tail in the momentum distribution or in RF spectroscopy. The fast decay due to the higher power law in these latter two cases imposes very stringent signal-to-noise requirements for a given range of momentum or frequency. As we have already shown before, experimentally, the static structure factor $S(q) = S_{\uparrow\uparrow}(q) + S_{\uparrow\downarrow}(q)$ can be readily measured using two-photon Bragg spectroscopy on a balanced two-component atomic Fermi gas near a Feshbach resonance. In the large-q limit, to a good approximation, $S_{\uparrow\uparrow}(q) \simeq 1$. One thus can directly determine the spin-antiparallel SSF $S_{\uparrow\downarrow}(q) = S(q) - 1$ and verify the simple $1/q$ asymptotic behavior.

In Fig. 8, we show the experimental confirmation of Eq. (27) at lowest experimental temperatures [38]. The SSF has been measured as a function of the inverse transferred momentum k_F/q at three interaction parameters, shown by the symbols with error bars [38]. The solid lines plot the theoretical prediction of Eq. (27). The contact $\mathcal{I}$ used in the equation has been calculated by using Tan's adiabatic relation and the reliable theoretical results for zero-temperature equation of state [55]. The agreement between theory and experiment is quantitative. At $1/(k_Fa) = +0.3$, the data depart from a straight line displaying the downward curvature consistent with the first order term in Eq. (27). A similar upward curvature is seen at $1/(k_Fa) = -0.2$. The simple structure-factor Tan relation is seen to accurately describe the SSF in the BEC–BCS crossover demonstrating the wide

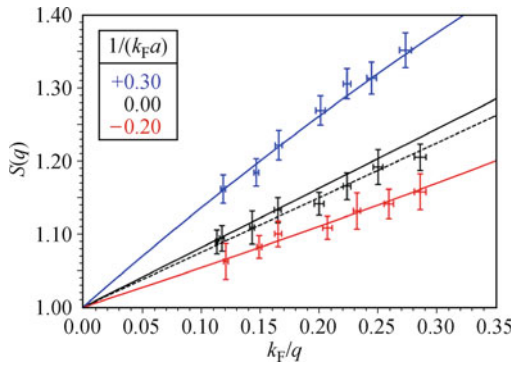

Fig. 8 Experimental confirmation of the structure-factor Tan relation Eq. (27). The measured static structure factor of a trapped crossover Fermi gas at lowest attainable temperature is plotted as a function of inverse transferred wave-vector. The solid lines show the theoretical prediction of Eq. (27). The dashed line is a linear fit to the experimental data in the unitary limit. It lies slightly below the predicted solid line, presumably due to the finite temperature effect [38]. Reproduced from Ref. [38], Copyright © 2010 American Physical Society.

applicability of the Tan relations.

Using Eq. (27), we are able to measure experimentally the contact at both low temperature and finite temperature [39, 40]. In Figs. 9(a) and (b), we report respectively the contact as a function of the dimensionless interaction parameter at zero temperature and as a function of temperature in the unitary limit. The experimental data are compared with the theoretical predictions from strong-coupling pair-fluctuation theory [55]. At high temperature, we also show the virial expansion prediction for the contact [55]. In all cases, the agreement between theory and experiment is excellent.

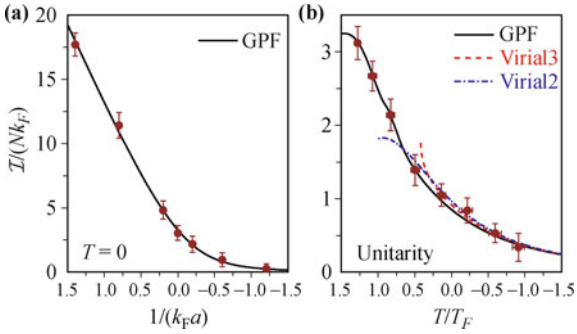

Fig. 9 **(a)** Measured contact of a trapped Fermi gas in the BEC–BCS crossover at lowest experimental temperature. **(b)** Temperature dependence of the universal contact of the trapped unitary Fermi gas in traps. In both plots, the solid lines are the theoretical prediction from a pair-fluctuation theory [55]. The dashed and dashed-dotted lines in (b) are the virial expansion predictions up to the third and second order, respectively. The experimental data are taken from Refs. [39] and [40], Copyright © 2011 American Physical Society and Copyright © 2011 Institute of Physics respectively.

5.2 High-frequency tail of DSF at large momentum

We now turn to consider the high-frequency tail of DSF at large momentum. At zero temperature, the large-q and large-ω behavior of DSF may be calculated using Feynman diagrams [59, 60]. In the upper panel of Fig. 10, we sketch the leading diagrams to $\chi_{\sigma\sigma'}(\boldsymbol{q},\omega)$ in the limit of $(\boldsymbol{q},\omega)\to\infty$. Diagrammatically, the contact may be identified as the vertex function at short distance and time [55]: $\mathcal{I}=-m^2\Gamma(\boldsymbol{r}=\boldsymbol{0},\tau=0^-)/\hbar^4$. Therefore, in the diagrams the shadow part of the vertex function $\Gamma(\boldsymbol{r}=\boldsymbol{0},\tau=0^-)$ represents the contact $\mathcal{I}$. These diagrams are well-known in condensed matter community. In the context of calculating the change in conductivity due to conducting fluctuations, the last two diagrams are called the Maki–Thompson (MT) [62, 63] and Aslamazov–Larkin (AL) [64] contributions, respectively, while the first diagram gives the self-energy (S) correction. At zero temperature, we calculate these diagrams in vacuum at $\mu=0$ and obtain that $S_{\uparrow\uparrow}^{T=0}=\mathcal{I}(f_S-f_{\rm AL})/(4\pi^2\sqrt{m\hbar}\omega^{3/2})$ and $S_{\uparrow\downarrow}^{T=0}=\mathcal{I}(f_{\rm MT}-f_{\rm AL})/(4\pi^2\sqrt{m\hbar}\omega^{3/2})$, where

$$f_S=\frac{\sqrt{1-x/2}}{(1-x)^2} \tag{28}$$

$$f_{\rm MT}=\frac{1}{\sqrt{2x}}\ln\frac{1+\sqrt{2x-x^2}}{|1-x|} \tag{29}$$

$$f_{\rm AL}=\frac{1}{2x\sqrt{1-x/2}}\left[\ln^2\frac{1+\sqrt{2x-x^2}}{|1-x|}-\pi^2\Theta(x-1)\right] \tag{30}$$

$x\equiv\hbar^2\boldsymbol{q}^2/(2m\hbar\omega)$, and Θ is the step function. These results agree with the previous calculations by Son and Thompson [60], although therein the spin parallel and antiparallel DSFs were not treated separately. At small $\boldsymbol{q}^2/\omega$, we find that the spin parallel and antiparallel DSFs have the tail

$$S_{\uparrow\uparrow}^{T=0}=-S_{\uparrow\downarrow}^{T=0}=\frac{\hbar^{1/2}\boldsymbol{q}^2}{12\pi^2m^{3/2}\omega^{5/2}}\mathcal{I} \tag{31}$$

This prediction shows that for $\omega\to\infty$ the spin dependent DSFs decay an order slower in magnitude than the total DSF. The latter is proportional to $q^4/\omega^{7/2}$, as shown in Refs. [60] and [61]. The faster decay in the total dynamic structure factor is due to the cancellation of the leading terms in $S_{\uparrow\uparrow}^{T=0}$ and $S_{\uparrow\downarrow}^{T=0}$.

In the lower panel of Fig. 10, we show the virial expansion prediction for the DSF at $T=0.5T_{\rm F}$ and $1/(k_Fa)=1.0$. The high-frequency tail is clearly evident after we multiply $\omega^{7/2}$ and $\omega^{5/2}$ to the total DSF and the spin-antiparallel DSF. It follows the prediction of Eq. (31), as shown by the dot-dashed lines. For the spin-antiparallel DSF, the asymptotic tail is reached at $\omega\sim 2\omega_R$. This frequency regime is indeed experimentally attainable.

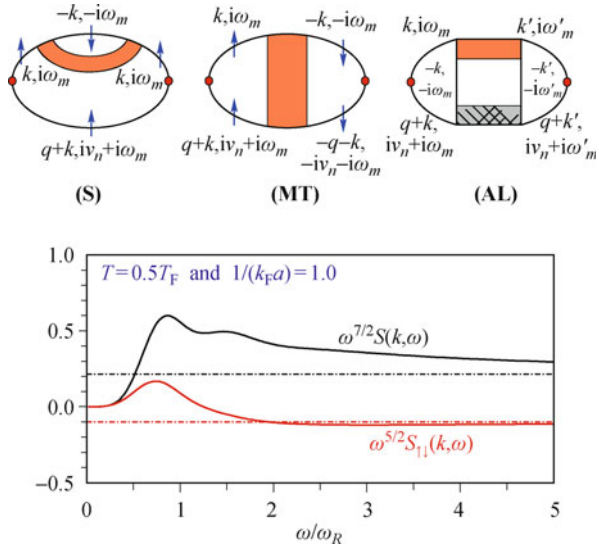

Fig. 10 *Upper panel*: Leading diagrammatic contributions to the dynamic susceptibility in the limits of large momentum and frequency. The self-energy (S) and Maki–Thompson (MT) diagrams contribute to $\Delta\chi_{\uparrow\uparrow}(\boldsymbol{r},\tau)$ and $\Delta\chi_{\uparrow\downarrow}(\boldsymbol{r},\tau)$, respectively, while the Aslamazo–Larkin diagram (AL) contributes to both. The shadow in the diagrams represents the contact $\mathcal{I}$. The crossed part in the diagram (AL) is the vertex. *Lower panel*: Asymptotic large-frequency tail of the total and spin-antiparallel dynamic structure factor at $T=0.5T_{\rm F}$ and $1/(k_Fa)=1$. Here, the transferred wavevector is $q=2.7k_{\rm F}$. Reproduced from Ref. [59] with permission.

6 Conclusions

In summary, we have reviewed several theoretical approaches for understanding the dynamic structure factor of a strongly correlated Fermi gas [32–34]. The resultant theoretical predictions agree quantitatively well with the current experimental data from Bragg spectroscopy at a large transferred momentum [28, 38–40]. The pros and cons of different theoretical tools may be commented as follows.

(1) The strong-coupling RPA theory is perturbative. This theory is quantitatively applicable at low temperature and large transferred momentum, as confirmed by the excellent agreement with the experimental Bragg spectra [32]. It is most likely valid in a narrow temperature window near $T = 0$. With increasing temperature, the pairing gap decreases and thermal pair fluctuations increase. It will eventually break down at a characteristic temperature $T_{\rm RPA}(\lesssim T_c)$. The applicability of RPA theory at small momentum is to be checked.

(2) The quantum virial expansion is non-perturbative. It is quantitatively applicable at temperature $T \gtrsim T_{\rm F}$ for arbitrary transferred momentum. By including higher-order virial expansion functions, it is appealing to extend the virial expansion closer to the superfluid transition temperature [33]. The virial theory is also efficient for investigating other basic dynamical properties, such as the spectral function of single-particle Green function [54]. It provides a benchmark for testing strong-coupling theories at high temperatures.

(3) The asymptotic Tan relations are non-perturbative. It is exact but is restricted to large transferred momentum [34]. It gives us a test-bed for strong-coupling theories at large momentum and large frequency.

The combined use of different theoretical approaches may give us insights on future development of strong-coupling theories for dynamic structure factor. From the virial expansion approach, we may learn how to include the few-particle correlations in the strong-coupling theories. On the other hand, as we have shown in Section 5.2, the Tan relation may be obtained by classifying the Feynman diagrams at the leading order of $1/q$ and $1/\omega$ [59]. It is interesting to develop a novel strong-coupling theory by including Feynman diagrams at the different orders of $1/q$ and $1/\omega$.

Acknowledgements We acknowledge valuable contributions from Xia-Ji Liu, Peter D. Drummond, Peng Zou, Eva D. Kuhnle, Chris J. Vale, and Peter Hannaford. This work was supported by the ARC Discovery Project No. DP0984522 and the NFRP-China Grant No. 2011CB921502.

References

1. I. Bloch, J. Dalibard, and W. Zwerger, Rev. Mod. Phys., 2008, 80(3): 885
2. S. Giorgini, L. P. Pitaevskii, and S. Stringari, Rev. Mod. Phys., 2008, 80(4): 1215
3. T. L. Ho, Phys. Rev. Lett., 2004, 92(9): 090402
4. H. Hu, P. D. Drummond, and X. J. Liu, Nat. Phys., 2007, 3(7): 469
5. K. M. O'Hara, S. L. Hemmer, M. E. Gehm, S. R. Granade, and J. E. Thomas, Science, 2002, 298(5601): 2179
6. C. Chin, M. Bartenstein, A. Altmeyer, S. Riedl, S. Jochim, J. Hecker Denschlag, and R. Grimm, Science, 2003, 305(5687): 1128
7. J. Kinast, S. L. Hemmer, M. E. Gehm, A. Turlapov, and J. E. Thomas, Phys. Rev. Lett., 2004, 92(15): 150402
8. M. Bartenstein, A. Altmeyer, S. Riedl, S. Jochim, C. Chin, J. H. Denschlag, and R. Grimm, Phys. Rev. Lett., 2004, 92(20): 203201
9. H. Hu, A. Minguzzi, X. J. Liu, and M. P. Tosi, Phys. Rev. Lett., 2004, 93(19): 190403
10. C. A. Regal, M. Greiner, and D. S. Jin, Phys. Rev. Lett., 2004, 92(4): 040403
11. M. W. Zwierlein, C. A. Stan, C. H. Schunck, S. M. F. Raupach, A. J. Kerman, and W. Ketterle, Phys. Rev. Lett., 2004, 92(12): 120403
12. M. W. Zwierlein, J. R. Abo-Shaeer, A. Schirotzek, C. H. Schunck, and W. Ketterle, Nature, 2005, 435(7045): 1047
13. J. T. Steward, J. P. Gaebler, C. A. Regal, and D. S. Jin, Phys. Rev. Lett., 2006, 97: 220406
14. L. Luo, B. Clancy, J. Joseph, J. Kinast, and J. E. Thomas, Phys. Rev. Lett., 2007, 98(8): 080402
15. S. Nascimbène, N. Navon, K. J. Jiang, F. Chevy, and C. Salomon, Nature, 2010, 463(7284): 1057
16. H. Hu, X. J. Liu, and P. D. Drummond, New J. Phys., 2010, 12(6): 063038
17. H. Hu, X. J. Liu, and P. D. Drummond, Phys. Rev. A, 2008, 77(6): 061605 (R)
18. G. E. Astrakharchik, J. Boronat, J. Casulleras, and A. S. Giorgini, Phys. Rev. Lett., 2004, 93(20): 200404
19. A. Bulgac, J. E. Drut, and P. Magierski, Phys. Rev. Lett., 2006, 96(9): 090404
20. E. Burovski, E. Kozik, N. Prokof'ev, B. Svistunov, and M. Troyer, Phys. Rev. Lett., 2008, 101(9): 090402
21. V. K. Akkineni, D. M. Ceperley, and N. Trivedi, Phys. Rev. B, 2007, 76(16): 165116
22. J. Carlson and S. Reddy, Phys. Rev. Lett., 2008, 100(15): 150403
23. Y. Ohashi and A. Griffin, Phys. Rev. Lett., 2002, 89(13): 130402
24. Y. Ohashi and A. Griffin, Phys. Rev. A, 2003, 67(6): 063612
25. H. Hu, X. J. Liu, and P. D. Drummond, Europhys. Lett., 2006, 74(4): 574
26. R. Haussmann, W. Rantner, S. Cerrito, and W. Zwerger, Phys. Rev. A, 2007, 75(2): 023610
27. J. T. Stewart, J. P. Gaebler, and D. S. Jin, Nature, 2008, 454(7205): 744
28. G. Veeravalli, E. D. Kuhnle, P. Dyke, and C. J. Vale, Phys. Rev. Lett., 2008, 101(25): 250403
29. A. Griffin, Excitations in a Bose-Condensed Liquid, New York: Cambridge, 1993
30. A. L. Fetter and J. D. Walecka, Quantum Theory of Many-Particle Systems, New York: McGraw-Hill, 1971

31. D. M. Stamper-Kurn, A. P. Chikkatur, A. Görlitz, S. Inouye, S. Gupta, D. E. Pritchard, and W. Ketterle, Phys. Rev. Lett., 1999, 83(15): 2876
32. P. Zou, E. D. Kuhnle, C. J. Vale, and H. Hu, Phys. Rev. A, 2010, 82(6): 061605 (R)
33. H. Hu, X. J. Liu, and P. D. Drummond, Phys. Rev. A, 2010, 81(3): 033630
34. H. Hu, X. J. Liu, and P. D. Drummond, Europhys. Lett., 2010, 91(2): 20005
35. S. Tan, Ann. Phys., 2008, 323(12): 2952
36. S. Tan, Ann. Phys., 2008, 323(12): 2971
37. S. Tan, Ann. Phys., 2008, 323(12): 2987
38. E. D. Kuhnle, H. Hu, X. J. Liu, P. Dyke, M. Mark, P. D. Drummond, P. Hannaford, and C. J. Vale, Phys. Rev. Lett., 2010, 105(7): 070402
39. E. D. Kuhnle, S. Hoinka, P. Dyke, H. Hu, P. Hannaford, and C. J. Vale, Phys. Rev. Lett., 2011, 106(17): 170402
40. E. D. Kuhnle, S. Hoinka, H. Hu, P. Dyke, P. Hannaford, and C. J. Vale, New J. Phys., 2011, 13(5): 055010
41. R. Combescot, S. Giorgini, and S. Stringari, Europhys. Lett., 2006, 75(5): 695
42. A. Minguzzi, G. Ferrari, and Y. Castin, Eur. Phys. J. D, 2001, 17(1): 49
43. G. M. Bruun and B. R. Mottelson, Phys. Rev. Lett., 2001, 87: 270403
44. R. Combescot, M. Yu. Kagan, and S. Stringari, Phys. Rev. A, 2006, 74(4): 042717
45. X. J. Liu and H. Hu, Phys. Rev. A, 2005, 72(6): 063613
46. X. J. Liu, H. Hu, A. Minguzzi, and M. P. Tosi, Phys. Rev. A, 2004, 69(4): 043605
47. S. Stringari, Phys. Rev. Lett., 2009, 102(11): 110406
48. X. J. Liu, M. Modugno, and H. Hu, Phys. Rev. A, 2003, 68(5): 053605
49. X. J. Liu, H. Hu, and P. D. Drummond, Phys. Rev. A, 2007, 75(2): 023614
50. T. L. Ho and E. J. Mueller, Phys. Rev. Lett., 2004, 92(16): 160404
51. X. J. Liu, H. Hu, and P. D. Drummond, Phys. Rev. Lett., 2009, 102(16): 160401
52. X. J. Liu, H. Hu, and P. D. Drummond, Phys. Rev. A, 2010, 82(2): 023619
53. X. J. Liu, H. Hu, and P. D. Drummond, Phys. Rev. B, 2010, 82(5): 054524
54. H. Hu, X. J. Liu, P. D. Drummond, and H. Dong, Phys. Rev. Lett., 2010, 104(24): 240407
55. H. Hu, X. J. Liu, and P. D. Drummond, New J. Phys., 2011, 13(3): 035007
56. M. Punk and W. Zwerger, Phys. Rev. Lett., 2007, 99(17): 170404
57. G. Baym, C. J. Pethick, Z. Yu, and M. W. Zwierlein, Phys. Rev. Lett., 2007, 99(19): 190407
58. E. Braaten and L. Platter, Phys. Rev. Lett., 2008, 100(20): 205301
59. H. Hu and X. J. Liu, arXiv:1101.1134, 2011
60. D. T. Son and E. G. Thompson, Phys. Rev. A, 2010, 81(6): 063634
61. E. Taylor and M. Randeria, Phys. Rev. A, 2010, 81(5): 053610
62. K. Maki, Prog. Theor. Phys., 1968, 40(2): 193
63. R. S. Thompson, Phys. Rev. B, 1970, 1(1): 327
64. L. G. Aslamazov and A. I. Larkin, Phys. Lett. A, 1968, 26: 238